



Time-Dependent Density Functional Theory for Atomic Collisions: A Progress Report

Tom Kirchner



Department of Physics and Astronomy, York University, Toronto, ON M3J 1P3, Canada; tomk@yorku.ca

Abstract: In this paper, the current status of time-dependent density functional theory (TDDFT)based calculations for ion-atom collision problems is reviewed. Most if not all reported calculations rely on the semiclassical approximation of heavy particle collision physics and the time-dependent Kohn-Sham (TDKS) scheme for computing the electronic density of the system. According to the foundational Runge-Gross theorem, all information available about the electronic many-body system is encoded in the density; however, in practice it is often not known how to extract it without resorting to modelling and approximations. This is in addition to a necessarily approximate implementation of the TDKS scheme due to the lack of precise knowledge about the potential that drives the equations. Notwithstanding these limitations, an impressive body of work has been accumulated over the past few decades. A sample of the results obtained for various collision systems is discussed here, in addition to the formal underpinnings and theoretical and practical challenges of the application of TDDFT to atomic collision problems, which are expounded in mostly nontechnical terms. Open problems and potential future directions are outlined as well.

Keywords: time-dependent density functional theory; ion-atom collisions; semiclassical approximation; time-dependent Kohn-Sham scheme; independent electron model; correlation integral

1. Introduction

Time-dependent density functional theory (TDDFT) was established as a formally exact framework for the discussion of time-dependent many-body problems by Runge and Gross in a landmark foundational paper 40 years ago [1]. While formal in scope and execution, their work took inspiration from a nascent practical interest in treating timedependent problems such as atomic collisions in terms of density functionals. Interestingly, it took until the late 1990s for systematic TDDFT-based computational studies of manyelectron collision systems to emerge [2–5]. This is similar to the situation in the related field of strong laser field interactions with atoms, in which the TDDFT approach took off as a practical tool just a few years earlier [6–9]. The considerable time gap between the foundation and execution of TDDFT in the nonlinear response regime is a reflection of two problems: (i) the Runge–Gross theorem of [1] does not provide all the ingredients needed for setting up a practical calculation; and (ii) practical schemes based on high-quality ingredients established in subsequent works turned out to be computationally demanding.

For collision studies, the latter problem is exacerbated by a lack of symmetries that can be exploited and the inherent two-center nature of problems involving a positively charged projectile ion that can capture target atom electrons in addition to promoting them to excited bound and continuum states. As a matter of fact, the community has struggled to reach agreement even on the most basic one-electron ion-atom scattering problem, namely, the proton-hydrogen system, for which one does not need TDDFT or any other many-body approach. Only recently has this changed, with consensus being reported regarding the magnitude of the total ionization cross-section in the intermediate energy region, where it peaks and competes with capture and target excitation [10].



Citation: Kirchner, T. Time-Dependent Density Functional Theory for Atomic Collisions: A Progress Report. Atoms 2024, 12, 31. https://doi.org/ 10.3390/atoms12060031

Academic Editor: David D. Reid

Received: 3 May 2024 Revised: 24 May 2024 Accepted: 27 May 2024 Published: 1 June 2024



Copyright: © 2024 by the author. Licensee MDPI, Basel, Switzerland This article is an open access article distributed under the terms and conditions of the Creative Commons Attribution (CC BY) license (https:// creativecommons.org/licenses/by/ 4.0/).

Atoms **2024**, 12, 31 2 of 25

The promise of TDDFT is that a full solution of a time-dependent many-body problem is possible, at least in principle, without determination of the state vector. The Runge–Gross theorem establishes that the one-particle density, a function of three spatial coordinates and time, suffices to extract all information, and can be obtained from solving a set of effective single-particle equations, that is, the time-dependent Kohn–Sham (TDKS) equations. Contrasting this with the multidimensional time-dependent Schrödinger equation (TDSE) for the state vector, this approach sounds like an enormous simplification; however, there is a hitch. The Runge–Gross theorem has the form of an existence theorem, and, as alluded to above, does not come with prescriptions for how to determine the exact form of important quantities such as the single-particle potential that drives the TDKS equations or many observables of interest. As a consequence, it is necessary to resort to models and approximations in order to turn TDDFT into a workable scheme for practical applications.

The present article attempts to assess the current status of TDDFT as a viable approach to the solution of many-electron collision problems which can be discussed within the semiclassical approximation. Semiclassical here means that the heavy particles (nuclei) are assumed to move on classical trajectories, with only the electrons following the laws of quantum mechanics. In some ways, this paper can be seen as an update of (the more theoretical) Chapter 12 and (the more practical) Chapter 24 of the book [11], published some twenty years ago, although it is not our intention to be comprehensive and review all works published since. Rather, the goal is to illustrate what can and cannot be done with current TDDFT methods so as to provide some pointers for prospective and desirable future developments. The focus is on collisions involving *atoms*, which is well-suited to outlining the main accomplishments and remaining difficulties and is in line with the theme of this special issue, although much of the current activity in the field is concerned with larger objects such as molecules and clusters.

The theoretical underpinnings of TDDFT have not changed since the publication of [11]. Considering that book's Chapter 12 and the availability of other books [12,13] and review articles [14] on TDDFT, a condensed and rather nontechnical summary of the main concepts should suffice for our purposes. Section 2 provides that summary, covering the contents of the Runge–Gross theorem (Section 2.1), available options for the TDKS potential (Section 2.2), and a somewhat more detailed discussion of open problems related to the calculation of the observables of interest (Section 2.3). These problems can be best exemplified for *two* electrons; hence, this case receives special attention in Section 2.3.3, following brief discussions of known exact observable functionals (Section 2.3.1) and functionals at the independent electron model (IEM) level (Section 2.3.2). Section 3 presents an overview of recent results obtained for various observables and collision systems, including negatively and positively charged projectiles. The paper ends with a few summarizing remarks, including a brief outlook on potential future research directions in Section 4. Atomic units, characterized by $\hbar = m_e = e = 4\pi\epsilon_0 = 1$, are used unless otherwise stated.

2. Theoretical Considerations

The evolution of a nonrelativistic many-body system driven by a Hamiltonian that may explicitly depend on time is governed by the TDSE

$$(\hat{H}(t) - i\partial_t)\Psi(t) = 0, \tag{1}$$

to be solved for some given initial state $\Psi(t_0) = \Psi_0$. We are interested in systems of interacting electrons which, in addition to their (time-independent) mutual Coulomb repulsion, experience Coulomb fields associated with stationary and/or classically moving nuclei. For ion–atom collisions at collision energies above, say, 1 keV/amu, simple straightline projectile trajectories characterized by an impact parameter b and constant speed v are known to represent the situation very well [15]. At lower energies or for molecular systems and clusters which may rearrange or dissociate upon the ion impact induced electron dynamics, it is possible to go beyond the simple recipe of prescribed (linear) trajectories and couple the quantum mechanical electron motion with classical nuclear dynamics, e.g., by using

Atoms 2024, 12, 31 3 of 25

the so-called Ehrenfest dynamics approach (see, e.g., Chapter 17 of the book [13]). In any case, within the semiclassical approximation, the Hamiltonian in Equation (1) consists of the kinetic energy operator \hat{T} of the electrons, the universal electron–electron repulsion \hat{V}_{ee} , and the system-specific external potential $\hat{V}_{\text{ext}}(t)$:

$$\hat{H}(t) = \hat{T} + \hat{V}_{ee} + \hat{V}_{ext}(t)
= \sum_{j=1}^{N} \left(-\frac{1}{2} \nabla_{j}^{2} \right) + \sum_{i < j}^{N} \frac{1}{|\mathbf{r}_{i} - \mathbf{r}_{j}|} + \sum_{j=1}^{N} v_{ext}(\mathbf{r}_{j}, t).$$
(2)

For an ion–atom collision system, we can write for the external single-electron potentials in Equation (2):

 $v_{\text{ext}}(\mathbf{r},t) = -\frac{Z_T}{r} - \frac{Z_P}{|\mathbf{r} - \mathbf{R}(t)|}$ (3)

where Z_T and Z_P are the atomic charge numbers of the target and projectile nuclei. The target nucleus is placed at the origin of the reference frame, and for sufficiently high collision energies the projectile position vector takes the simple straightline form $\mathbf{R}(t) = (b, 0, vt)$.

It is not impossible to attack this time-dependent many-electron problem directly, e.g., by a correlated configuration-interaction approach based on an atomic orbital expansion. In practice, such explicit many-electron approaches are mostly restricted to collision systems with two and three active electrons, and become prohibitively expensive for larger electron numbers N. An example of a recent state-of-the-art three-electron calculation can be found in [16], and a compact overview of existing full and approximate many-electron methods is provided in the handbook chapter [17].

2.1. TDDFT Foundations

TDDFT is based on the rather nonintuitve insight that the solution of the TDSE (1) is fully encoded in the time-dependent density of the *N*-electron system

$$n(\mathbf{r},t) = N \sum_{\sigma_1 \dots \sigma_N} \int d^3 r_2 \dots d^3 r_N |\Psi(\mathbf{r},\sigma_1,\mathbf{r}_2,\sigma_2,\dots,\mathbf{r}_N,\sigma_N,t)|^2, \tag{4}$$

where \mathbf{r}_k , σ_k are the position and spin of the kth electron with $\sigma_k = \uparrow, \downarrow$. The density is a measure of the electronic charge distribution, and is normalized to the total number of electrons

$$\int n(\mathbf{r},t)d^3r = N,\tag{5}$$

which corresponds to the statement that the total charge is *N* times the (negative) elementary charge constant.

In more technical terms, the Runge–Gross theorem establishes that, for a given initial state and up to a purely time-dependent phase factor, $\Psi(t)$ is a unique functional of n: $\Psi = \Psi[n](t)$. This has the immediate consequence that any observable that can be written as an expectation value of some operator \hat{O} is a functional of n as well:

$$O(t) \equiv \langle \Psi[n](t)|\hat{O}(t)|\Psi[n](t)\rangle = O[n](t). \tag{6}$$

In other words, any such observable is determined by the density alone. This was proven by Runge and Gross for rather general situations. Paralleling the argumentation of stationary ground-state DFT, they proceeded to show that the density can be obtained from solving single-particle equations, that is, the TDKS equations¹

$$i\partial_t \psi_i(\mathbf{r}, t) = \left(-\frac{1}{2}\nabla^2 + v_{\text{TDKS}}[n](\mathbf{r}, t)\right)\psi_i(\mathbf{r}, t), \quad i = 1, \dots, N,$$
 (7)

Atoms 2024, 12, 31 4 of 25

by adding up the orbital densities

$$n(\mathbf{r},t) = \sum_{i=1}^{N} |\psi_i(\mathbf{r},t)|^2.$$
 (8)

As indicated, the TDKS potential $v_{\rm TDKS}$ is also a (unique) functional of n. If its exact form and the exact density dependence of all observables of interest were known, it would be possible to determine all the relevant properties of an interacting quantum system without solving the complicated many-body TDSE (1). In reality, however, most of these density functionals are unknown, and we must content ourselves with models and approximations in practical applications of TDDFT.

2.2. Approximate TDKS Potentials

The TDKS potential is usually decomposed into several pieces, thereby locating and specifying the unknown part. The most obvious known piece is the external potential (3); thus, what remains can be identified as being due to electron–electron interactions:

$$v_{\text{TDKS}}[n](\mathbf{r},t) \equiv v_{\text{ext}}(\mathbf{r},t) + v_{\text{ee}}[n](\mathbf{r},t). \tag{9}$$

Now, we have several options. The standard approach is to extract a classical potential, the so-called Hartree potential v_H , from v_{ee} and call the remaining piece the exchange-correlation potential v_{xc} :

$$v_{\text{ee}}[n](\mathbf{r},t) = v_H[n](\mathbf{r},t) + v_{xc}[n](\mathbf{r},t), \tag{10}$$

$$v_H[n](\mathbf{r},t) = \int \frac{n(\mathbf{r}',t)}{|\mathbf{r}-\mathbf{r}'|} d^3r'. \tag{11}$$

The Hartree potential, which accounts for the screening of the external potential by the electron cloud, is an explicit density functional. The unknown exchange correlation potential is a density functional as well; however, depending on the model used in practice, the n-dependence can be explicit or implicit. An important approach that takes advantage of the second option is the optimized potential method (OPM). In it, v_{xc} is made to depend on the TDKS orbitals explicitly, which in turn, by virtue of the Runge–Gross theorem, are density functionals [19,20]. It is known how to take exchange into account exactly in this framework [21], or, alternatively, with high accuracy when adopting the so-called Krieger–Li–Iafrate (KLI) approximation [21,22], which is easier to implement than the full OPM.

A popular example of the former option is the (adiabatic) local density approximation (ALDA), which is based on the density dependence of the homogeneous electron gas. While this is a seemingly inadequate model for an *inhomogeneous* atomic density, as the existing body of work indicates, it works quite well in certain circumstances, in particular when combined with a self-interaction correction scheme [23].

Both OPM and ALDA calculations are computationally demanding, the OPM even more so than the ALDA, and present problems associated with the nonlinearity of the evolution equations. Similar issues were first encountered and discussed in the context of the time-dependent Hartree–Fock (TDHF) method, and are often referred to collectively as the TDHF projection problem (cf. [24] and references therein). The projection problem can be avoided by resorting to a simpler class of models based on the decomposition

$$v_{\text{ee}}[n](\mathbf{r},t) = v_{\text{ee}}^{0}(r) + \delta v_{\text{ee}}[n](\mathbf{r},t), \tag{12}$$

where v_{ee}^0 is a ground-state potential (radially symmetric for atoms), which reflects the situation at asymptotic times before the collision of a bare projectile with an N-electron

Atoms 2024, 12, 31 5 of 25

atom. It can be determined using ground-state DFT, and should decay asymptotically like (N-1)/r, meaning that for the total target potential of a neutral atom $(Z_T = N)$ we have

$$-\frac{Z_T}{r} + v_{\text{ee}}^0(r) \xrightarrow{r \to \infty} -\frac{1}{r}.$$
 (13)

The "response potential" $\delta v_{\rm ee}$ accounts for the time-dependent changes in the electronelectron potential during the collision. In fast collisions or in situations in which one-electron transitions dominate strongly, it may be assumed that the no-response approximation

$$\delta v_{\rm ee}[n](\mathbf{r},t) = 0 \tag{14}$$

holds. If such conditions are not met, time-dependent screening effects can be modeled in a global fashion. The target response model introduced in [24] accounts for the increased attraction of the target potential as electron removal sets in during the collision via the ansatz

$$\delta v_{\text{ee}}(r,t) = f(P_{\text{net}}^{\text{rem}}(t))v_{\text{ee}}^{0}(r), \tag{15}$$

where $P_{\rm net}^{\rm rem}$ is the net electron removal (properly defined in Section 2.3.1) and f is some simple negative function, i.e., f < 0 for $P_{\rm net}^{\rm rem} > 0$, such that the total electron–electron potential (12), when taken together with the Coulomb potential of the target nucleus, acquires ionic character with fractional charge. No matter the exact form of f, a procedure that fixes the TDHF projection problem is known for the target response model [24]. Dynamic projectile response to account for changes in the effective projectile potential during multiple capture can be treated in a similar fashion [25].

The situation becomes more involved when dealing with a collision system in which, in addition to a number of electrons initially occupying orbitals of the target atom, projectile electrons participate actively, i.e., undergo transitions. Simple models of $\delta v_{\rm ee}$ do not have the flexibility to produce a total effective potential with the correct asymptotic behavior for all electrons involved, and approaches based on different potentials for target and projectile electrons so as to avoid this deficiency create other problems associated with losing the orthogonality of the TDKS orbitals. A systematic solution to all these issues can be attained by implementing a first-principles based approach, such as (a spin-dependent version of) the KLI method mentioned above, though at the price of more delicate numerics and higher computational cost [26].

2.3. Observables of Interest in Ion-Atom Collision Systems

Suppose that we knew the exact form of $v_{\rm ee}[n]$ and have the computational tools and means to solve the TDKS equations with high numerical accuracy; we would then have the exact electron density at our disposal. What experimentally accessible information about the collision system would this provide us with? The Runge–Gross theorem says that in principle all observables are determined (cf. Equation (6)); however, this does not answer the more practical question of how these observable functionals look like.

This subsection discusses the above problem at three levels. First, we look at a few observables that are directly related to the density, i.e., that can be calculated exactly. These quantities correspond to average electron numbers. Then, we briefly outline the standard approach to the calculation of less global observables at the level of the IEM. Next, we zero in on the two-electron problem, for which the limitations of the IEM are most obvious and well known. Finally, the so-called correlation integral is introduced as a tool for analyzing and potentially overcoming these limitations, in an approximate fashion, in practice.

2.3.1. Explicit Exact Density Functionals

One of the quantities whose exact density dependence is known is the energy loss of the projectile, or more precisely that part of it associated with the electronic excitations of Atoms 2024, 12, 31 6 of 25

the target system². It can be obtained by comparing the energy expectation value of the electronic system

$$\mathcal{E}(t) = \langle \Psi(t) | \hat{H}(t) | \Psi(t) \rangle \tag{16}$$

at a final time t_f and the initial time t_i , which characterize the situation long after and long before the collision, when projectile and target are far away from each other and their interaction can be neglected. We can write

$$\mathcal{E}_{L} \equiv \mathcal{E}(t_{f}) - \mathcal{E}(t_{i}) = \int_{t_{i}}^{t_{f}} \dot{\mathcal{E}}(t) dt$$
 (17)

and use Ehrenfest's theorem for the time derivative of expectation values of observables for the Hamiltonian of Equation (2):

$$\dot{\mathcal{E}}(t) = \langle \Psi(t) | \partial_t \hat{H}(t) | \Psi(t) \rangle = \langle \Psi(t) | \sum_{j=1}^N \dot{v}_{\text{ext}}(\mathbf{r}_j, t) | \Psi(t) \rangle = \int n(\mathbf{r}, t) \dot{v}_{\text{ext}}(\mathbf{r}, t) d^3 r.$$
 (18)

 \mathcal{E}_L is an explicit density functional, albeit one that depends on the density at all times during the collision.

Simpler explicit density functionals of practical interest are the so-called net electron numbers, which involve integrals of the density over disjoint regions in space at asymptotic times. Net electron removal, for example, can be defined as

$$P_{\text{net}}^{\text{rem}} = N - \int_{T} n(\mathbf{r}, t_f) d^3 r, \tag{19}$$

where T is a region around the target center that contains all bound-state contributions to n. If the projectile is a bare ion initially, we can define net electron capture analogously:

$$P_{\text{net}}^{\text{cap}} = \int_{\mathcal{D}} n(\mathbf{r}, t_f) d^3 r \tag{20}$$

and net ionization to the continuum as follows

$$P_{\text{net}}^{\text{ion}} = P_{\text{net}}^{\text{rem}} - P_{\text{net}}^{\text{cap}} = \int_{I} n(\mathbf{r}, t_f) d^3 r$$
 (21)

where $I = \mathbb{R}^3 \setminus (T \cup P)$.

2.3.2. Approximate Functionals at the IEM Level

Reference [28] explains how to express final-state observables, such as the probability of finding a certain number of electrons in the continuum or a number of electrons transferred to the projectile and detected in coincidence with a number of electrons in the continuum, in terms of q-particle densities, a concept introduced by Löwdin in 1955 [29]. The Runge–Gross theorem ensures that the q-particle densities are functionals of n; however, the exact forms of these functionals are not known. To make progress, we can assume that the N-electron state vector Ψ is a single Slater determinant or even a non-symmetrized product of the TDKS orbitals. This allows explicit expressions to be established for the q-particle densities in terms of elements of the one-particle density matrix, an analysis which can be carried out in practice. In fact, the concept of q-particle densities is unnecessary after making these crucial approximations; the N-particle density itself, i.e., the operator $\hat{\gamma}^N = |\Psi\rangle\langle\Psi|$, can readily be written in terms of the one-particle density matrix at the IEM level, and the quantities of interest can be obtained without further detours. To quote two well-known explicit results, in the simplest model, in which $\hat{\gamma}^N$ is approximated as

Atoms 2024, 12, 31 7 of 25

> a product of one-particle densities, for the probability of capturing k and simultaneously ionizing *l* electrons to the continuum $(k + l \le N)$ we obtain [30]

$$P_{kl}^{\text{IEM}} = \binom{N}{k+l} \binom{k+l}{l} p_{\text{cap}}^k p_{\text{ion}}^l (1 - p_{\text{cap}} - p_{\text{ion}})^{N-k-l}, \tag{22}$$

where $p_x = P_{\text{net}}^x / N$ for x = cap, ion, and for the more inclusive probability of removing q = k + l electrons from the target,

$$P_q^{\text{IEM}} = \binom{N}{q} p_{\text{rem}}^q (1 - p_{\text{rem}})^{N-q}, \tag{23}$$

where $p_{\text{rem}} = P_{\text{net}}^{\text{rem}}/N = p_{\text{cap}} + p_{\text{ion}}$. Equations (22) and (23) correspond to an analysis in which the antisymmetry of the N-electron state is ignored and orbital-specific information is either unavailable or averaged out, i.e., the probabilities p_x can be interpreted as average (effective) single-electron probabilities. Normalization is fulfilled, e.g., from Equation (23) we obtain $\sum_{a} P_{a}^{\text{IEM}} = 1$.

2.3.3. The Correlation Integral for the Two-Electron Problem

The IEM outlined in the previous subsection has a long and successful track record in ion-atom collision studies; however, it has several known limitations. Considering electron removal in a two-electron spin-singlet system, either zero, one, or two electrons can be removed in a collision event. Using the short-hand $p \equiv p_{\rm rem}$, Equation (23) yields

$$P_0^{\text{IEM}} = (1 - p)^2, (24)$$

$$P_1^{\text{IEM}} = 2p(1-p), \tag{25}$$

$$P_0^{\text{IEM}} = (1-p)^2,$$
 (24)
 $P_1^{\text{IEM}} = 2p(1-p),$ (25)
 $P_2^{\text{IEM}} = p^2,$ (26)

respectively, for the three channels. Obviously, the probabilities for one-electron and two-electron removal have a fixed relation

$$P_1^{\text{IEM}} = 2\sqrt{P_2^{\text{IEM}}} \left(1 - \sqrt{P_2^{\text{IEM}}} \right), \tag{27}$$

with the maximum $P_{1,\text{max}}^{\text{IEM}} = 0.5$ occurring together with $P_{2}^{\text{IEM}} = 0.25$. This cannot be correct in general, i.e., the full solution of the two-electron TDSE (1) allows for more freedom. This can be seen from the following. An explicit two-electron treatment of a spin-singlet system begins with recognizing that the solution of Equation (1) can be written as $\Psi = \tilde{\Psi} \chi$ with an antisymmetric spin function χ , then expressing the removal of zero, one, or two electrons by suitably integrating the spatial two-electron density $\rho(\mathbf{r}_1, \mathbf{r}_2, t_f) = |\tilde{\Psi}(\mathbf{r}_1, \mathbf{r}_2, t_f)|^2$ at the final time $t = t_f$ over the disjoint regions in space T and $C = \mathbb{R}^3 \setminus T$:

$$P_0 = \iint_T d^3 r_1 d^3 r_2 \rho(\mathbf{r}_1, \mathbf{r}_2, t_f), \qquad (28)$$

$$P_1 = 2 \int_T \int_C d^3 r_1 d^3 r_2 \, \rho(\mathbf{r}_1, \mathbf{r}_2, t_f), \tag{29}$$

$$P_2 = \iint_C d^3r_1 d^3r_2 \, \rho(\mathbf{r}_1, \mathbf{r}_2, t_f). \tag{30}$$

The condition $P_0 + P_1 + P_2 = 1$ is observed. Provided that the target region T contains all bound-state contributions, these formulae are exact, just as Equations (19)–(21) for the net electron numbers. There is no fixed relation between P_1 and P_2 .

Atoms 2024, 12, 31 8 of 25

Using the analogue of Equation (4) for the spatial two-electron density ρ , we can establish that

$$P_1 + 2P_2 = P_{\text{net}}^{\text{rem}} = 2p,$$
 (31)

which obviously also holds within the IEM and affirms that the net numbers are indeed average electron numbers. In a next step, we can link the exact expressions (28)–(30) for P_0 , P_1 and P_2 with their IEM counterparts by introducing the correlation integral [31]

$$I_c = 2P_0 - \frac{1}{2}(2 - P_{\text{net}}^{\text{rem}})^2 = 2(P_0 - (1 - p)^2)$$
(32)

to obtain

$$P_0 = (1-p)^2 + \frac{1}{2}I_c, (33)$$

$$P_1 = 2p(1-p) - I_c, (34)$$

$$P_2 = p^2 + \frac{1}{2}I_c. (35)$$

From Equations (33)–(35), it is readily found that

$$I_c = 2P_0P_2 - \frac{1}{2}P_1^2. (36)$$

All we have done so far is rewrite the exact expressions (28)–(30) for electron removal by introducing the correlation integral in such a way that it would be zero if the IEM were exact, i.e., I_c really measures the departure from the IEM. This raises two questions: (i) how does I_c look like for a prototypical collision problem? and (ii) how can it be modeled or approximated without knowledge of the exact solution of the problem?

The first question was studied in [32], in which configuration-interaction calculations for antiproton–helium and antiproton–molecular hydrogen collisions were carried out and I_c was calculated from P_0 , P_1 , P_2 using Equation (36). To address the second question, we can begin by rewriting Equation (32) as

$$I_c = \iint_T d^3 r_1 d^3 r_2 g_c(\mathbf{r}_1, \mathbf{r}_2, t_f) n(\mathbf{r}_1, t_f) n(\mathbf{r}_2, t_f)$$
(37)

with

$$g_c(\mathbf{r}_1, \mathbf{r}_2, t_f) \equiv g(\mathbf{r}_1, \mathbf{r}_2, t_f) - g_x(\mathbf{r}_1, \mathbf{r}_2, t_f) = \frac{2\rho(\mathbf{r}_1, \mathbf{r}_2, t_f)}{n(\mathbf{r}_1, t_f)n(\mathbf{r}_2, t_f)} - \frac{1}{2},$$
(38)

and then introducing approximations to the correlation contribution g_c of the pair correlation function g. The first such attempt was made in the context of laser-induced ionization of helium, and involved using parametrizations and models of $g_c[n]$ established previously for ground-state systems applied now to the time-dependent density, in the spirit of an adiabatic approximation [33]. This turned out to have only a small effect on the calculated probabilities, a result that was later understood to be a general feature of models in which g_c approaches zero in the long-range limit $|\mathbf{r}_1 - \mathbf{r}_2| \to \infty$, which is a desirable property in ground-state systems but obviously not in ionization problems [34].

An improved adiabatic model was introduced in [35]. It was later applied to antiproton-helium collisions [31] and extended to deal with coincident capture and ionization events in positively-charged ion collisions [36]. In it, the two-particle and one-particle densities in g_c are approximated by linear combinations of ground-state densities [35]. The model is a density functional insofar as the coefficients of these linear combinations are determined by the net removal (19); however, the two-particle ground state density of neutral helium and the ground state density of the singly-charged ion are needed as additional ingredients. The former can be viewed, if not calculated, as an implicit functional of the helium ground-state density, i.e., the initial condition of the collision problem; however, the latter does not

Atoms 2024, 12, 31 9 of 25

seem to have any relation to the density of the collision system. In practice, both quantities can be calculated independently from the collision problem and then fed into the analysis.

Other approximations, some similar to those of [33] and one consisting of scaling a coupling-constant average of *g* by a two-parameter fit function, were proposed and applied to the problem of single and double capture in proton collisions with neon and argon atoms in [37].

3. Discussion of Selected Results

We now look at a set of results obtained from (variants of) the models discussed in Section 2. The data shown here are taken from a number of recent papers, with a view to outlining typical trends and highlighting open problems as opposed to providing a comprehensive review.

3.1. Projectile Energy Loss and Net Removal, Capture, and Ionization Cross-Sections

We begin with the projectile energy loss discussed in Section 2.3.1. A cross-section, sometimes called the (electronic) stopping cross-section, is obtained by the usual integration over the impact parameter:

$$S_e = 2\pi \int_0^\infty b \mathcal{E}_L(b) db. \tag{39}$$

In [27], S_e was calculated for antiproton collisions from first- and second-row atoms using Equations (17) and (18) together with densities obtained from the no-response approximation and the simple target response model discussed in Section 2.2. Orbital propagation was achieved by using the basis generator method (BGM), which is a basis expansion method in terms of atomic orbitals and a set of pseudostates constructed in a specific way so as to achieve an efficient representation of the ionization continuum [38]. There is obviously no electron capture channel for antiproton collisions, i.e., target electron removal can be identified with ionization to the continuum. The BGM pseudobasis used in [27] has a one-center character and is time-independent, which simplifies the calculations.

In Figure 1, S_e is shown for a neon target. The response and no-response results are virtually identical at collision energies above 200 keV, and are only marginally different from each other at lower energies. More striking is how they both differ from the semiclassical convergent close-coupling (SC-CCC) calculation from [39]. That calculation, also based on an expansion technique in terms of (single-center) pseudostates, does not rely on Equations (17) and (18) to extract the energy loss, instead using a more traditional approach to directly represent the expectation value of the electronic Hamiltonian in the basis. It also ignores multielectron contributions, only taking the 2p shell of neon into account, i.e., it is associated with energy loss due to single-electron processes involving one of the initial Ne(2p) electrons. The appararent discrepancy between the BGM and CCC calculations indicates that multielectron processes do contribute to energy loss; unfortunately, neither calculation provides direct evidence for this. From the TDDFT standpoint adopted in [27], decomposition of energy loss into single-electron and multiple-electron processes is not straightforward, and in practice would involve additional approximations similar to those described in Section 2.3.2. On the other hand, extending the CCC calculation of [39] to deal with multi-electron contributions would amount to turning a single active electron into a multiconfiguration calculation, which is not at all a routine step for a collision problem, if feasible at all. Qualitative support for the above interpretation is derived from the fact that nonzero multiple-ionization cross-sections have been measured (and calculated) for the antiproton–neon system (see [27] and references cited therein), i.e., multielectron processes do occur. Stopping power measurements, on the other hand, are outstanding, and would be most welcome to settle the issue. We note that BGM and CCC energy loss calculations for the one-electron antiproton-hydrogen system agree to within 10% [27].

Figure 2 displays a comparison of the energy loss cross-sections obtained for antiproton collisions with hydrogen, helium, carbon, nitrogen, oxygen, and neon atoms (right panel)

Atoms 2024, 12, 31 10 of 25

along with a corresponding comparison of the net ionization cross-sections (left panel). All calculations are based on the target response model and the BGM [27].

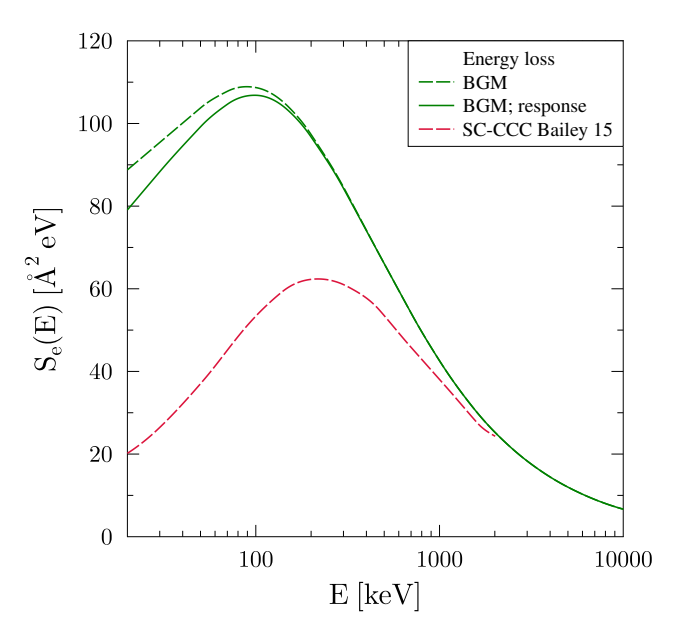


Figure 1. Energy loss cross-section for antiproton collisions with neon as a function of collision energy. The green dashed and solid lines represent the BGM calculations with static and dynamic response from [27]. The red-dashed energy loss curve is from the SC-CCC calculation of [39]. Reproduced with permission from [27].

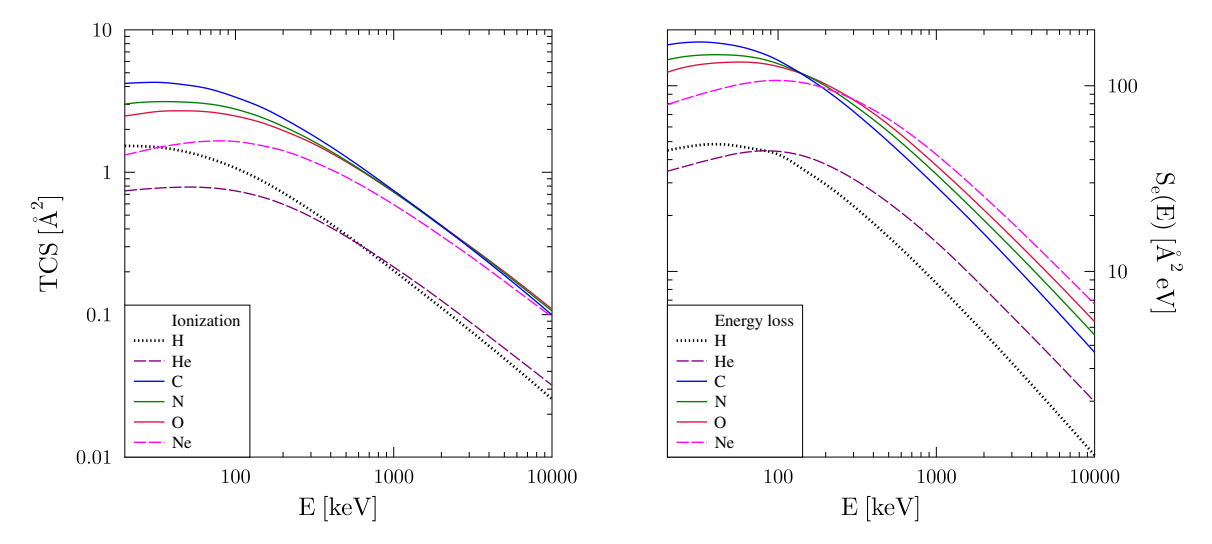


Figure 2. BGM response cross-sections for antiproton impact induced net ionization (**left panel**) and energy loss (**right panel**) for atoms of H (dotted black), He (dashed purple, close to H at high energies), C (solid blue), N (solid green), O (solid red), and Ne (dashed magenta) as functions of the collision energy. Reproduced with permission from [27].

The ordering of the energy loss and net ionization cross-sections is similar at low to intermediate collision energies, with helium at the bottom, followed by hydrogen, with which it crosses towards higher energies. The largest cross-sections are obtained for carbon, nitrogen, and oxygen, while neon is close to hydrogen in the case of net ionization, even falling below its cross-section at the lowest collision energies shown here, but rising towards the values for oxygen, nitrogen, and carbon in the case of energy loss before eventually surpassing them in the 200–300 keV impact energy range. There is no obvious common scaling of the results for either observable with the number of electrons and/or

Atoms 2024, 12, 31 11 of 25

the magnitude of the atomic ionization energies, although it is clear that both parameters play an important role in determining the cross-sections.

At higher impact energies, a grouping is observed more clearly for net ionization, for which hydrogen and helium remain at the bottom and are clearly separated from the rest while neon almost catches up with the data obtained for the other atoms, which basically land on a single curve. In the energy loss case, by contrast, neon emerges at the top, and the sequence of the cross-sections is strictly in accord with the number of electrons. In [27], it was shown for the quantity S_e/Z_T that the results for the (N>2) many-electron systems fall on a common curve at high energies, and that the hydrogen and helium results are close together and higher than this common curve.

Moving from antiprotons to positively charged projectiles opens up the electron capture channel, and in general requires the use of a two-center computational approach. An early TDDFT-based BGM calculation for net capture and net ionization in collisions of protons and He²⁺ ions with helium atoms was reported in [40]. Although it did not explicitly include bound projectile states in the basis, the (time-dependent) pseudostates had a two-center character, and capture probabilities were extracted from their population at asymptotic times using a projection technique. The effective electron–electron potential (10) was taken at the exchange-only level, i.e., correlation was neglected while exchange was included exactly. For helium, this is accomplished by multiplying the Hartree potential (11) by a factor of one half, as the elimination of the unphysical self-interaction contributions is the only role of exchange in this two-electron spin–singlet system.

Results for net capture and net ionization are shown in Figures 3 and 4, respectively. The exchange-only calculations (labeled as "response" in the figures) are compared with no-response results obtained using Equation (14) and with experimental data. As expected from the discussion in Section 2.2 (and see Figure 1), the two versions of theory agree with each other at high collision energies.

For the case of capture (Figure 3), an interesting difference is observed for proton vs. He²⁺ impact at low to intermediate energies. For the singly-charged projectile, the response results are below the no-response results; however, for the doubly-charged ion it is the other way around (below 20 keV/amu). In [40], this was explained with the aid of "dynamical correlation diagrams" obtained from diagonalizing the TDKS Hamiltonian in the BGM basis. For the (HeHe)²⁺ system, response effects bring the two potential curves relevant for ground-state electron transfer closer together, thereby increasing their coupling and the capture cross-section, while for the (HHe)⁺ system the energy gap between the potential curves widens so that capture becomes less likely. The experimental data displayed in the figure send a mixed message, as only in the case of the doubly-charged projectile does the inclusion of response appear to lead to better agreement. For proton impact, a more recent exchange-only level calculation [41] reported good agreement with the results of [40]. Calculations at the ALDA level appear to overestimate the capture cross-section at low collision energies [41,42]. A spin-dependent ALDA calculation with self-interaction corrections included, on the other hand, showed better agreement with the experimental data in the low-energy range [23]. State-resolved TDDFT capture results were reported in [43].

For the case of ionization (Figure 4), the theoretical situation is simpler. Response always reduces the cross-section, as it is associated with an increase in the binding of the electrons. The effect is relatively small, however, and comparison with the experimental data does not provide a clear-cut answer as to whether the response results are superior. In an ideal world in which the experimental data had negligible error bars and the theoretical results had exceedingly high numerical accuracy, it could be concluded from Figures 3 and 4 that any remaining discrepancy between theory and experiment would be resolved if we knew how to include correlation in the effective electron–electron potential (10).

Atoms **2024**, 12, 31 12 of 25

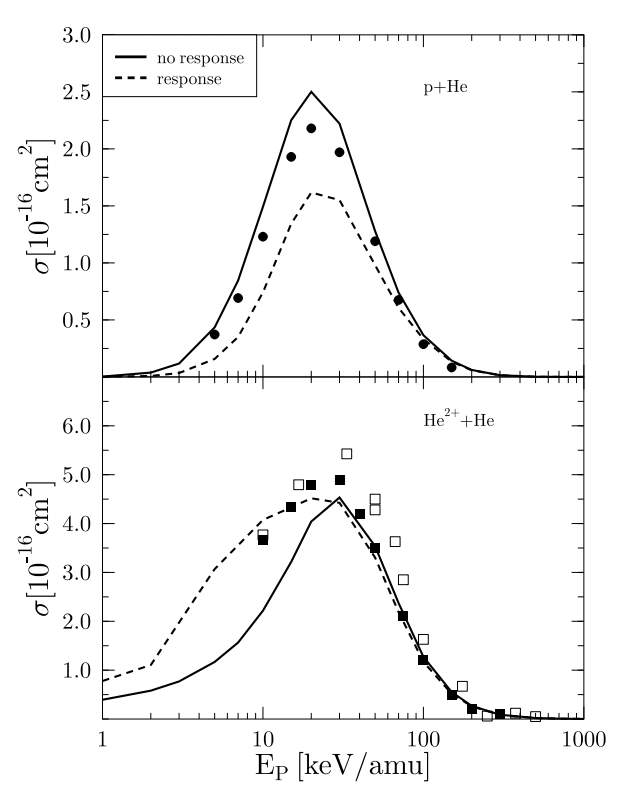


Figure 3. Total cross-sections for net capture in proton (**top**) and He^{2+} (**bottom**) collisions with helium as functions of collision energy. Curves: BGM calculations from [40]. Experiments: filled circles [44,45] (average deviation 8.8%); filled squares [46]; open squares [47,48]. Reproduced with permission from [40].

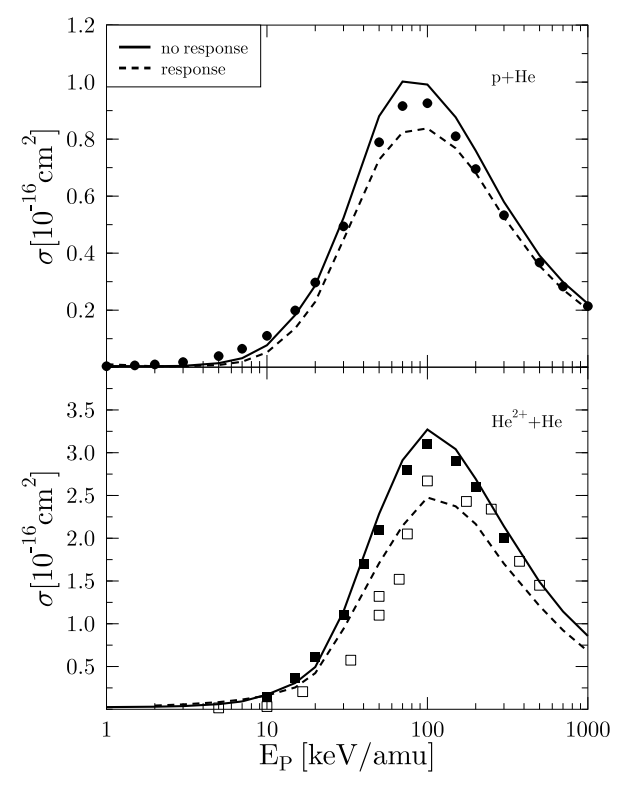


Figure 4. Total cross-sections for net ionization in proton (**top**) and He^{2+} (**bottom**) collisions with helium as functions of collision energy. Curves: BGM calculations from [40]. Experiments: filled circles [44,45] (average deviation 8.7%); filled squares [46] (uncertainty 80%); open squares [47,48] (typical uncertainties are $\pm 15\%$). Reproduced with permission from [40].

Atoms **2024**, 12, 31

3.2. Single-Electron and Double-Electron Processes in Collisions Involving Helium Atoms

The situation becomes more complicated when looking at, e.g., one-electron and two-electron removal, as opposed to net removal, in collisions involving helium atoms. As explained in Section 2, we face the problem that, in addition to the effective electron-electron potential, the observables have to be modeled or approximated. The available options are the IEM and, for the two-electron problem, one of the adiabatic correlation integral models described in Section 2.3.3. In Figure 5, the IEM and the adiabatic model proposed by Wilken and Bauer in [35] (labeled "WB" after the authors in the following text and figures) are compared for one-electron and two-electron removal in proton-helium and antiproton-helium collisions. The two plots are taken from [36], where results for proton-helium collisions for individual capture and ionization channels were shown and discussed in comparison with experimental data and other theoretical results. For the case of antiproton impact, a comparison with previous calculations was made in [31]. More recent (non-DFT) state-of-the-art studies of antiproton-helium collisions have been presented in [32,49,50].

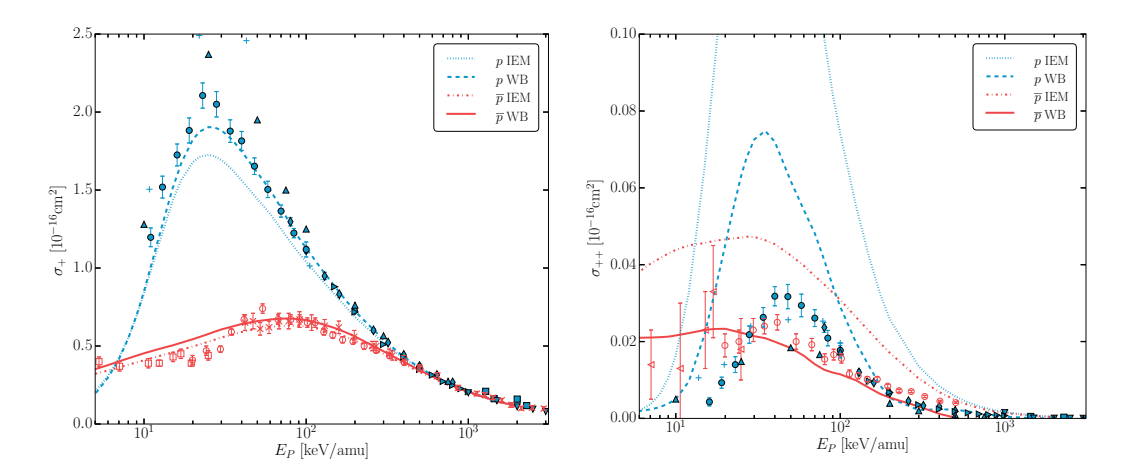


Figure 5. Total cross-sections for one-electron (left panel) and two-electron (right panel) removal from helium by proton and antiproton impact as functions of collision energy. Theory (BGM calculations from [36] with different final-state analyses): blue dotted lines, IEM for proton impact; red dash-dotted lines, IEM for antiproton impact; blue dashed lines, WB for proton impact; red solid lines, WB for antiproton impact. Experiments for proton impact: filled triangles [51], pluses [52], filled circles [53], filled diamonds [54], filled rightward triangles [55], filled downward triangles [56], filled squares [57]. Experiments for antiproton impact: open squares [58], open circles [59], crosses [60]. Reproduced with permission from [36].

The theoretical results displayed in Figure 5 were again obtained from BGM calculations. In addition to exact time-dependent screening and exchange contributions, the effective electron–electron potential (10) used here includes an accurate ground state correlation potential determined numerically by an inversion procedure [31]. The correlation potential was found to be unimportant for the collision calculations; thus, the single-particle solutions are in fact very similar to the exchange-only results (cf. Figures 3 and 4 for proton impact).

For both projectiles, the WB model enhances single removal (left panel) at the expense of double removal (right panel). Overall, this represents an improvement compared to the IEM, which shows very clear deficiencies in the case of double removal for both projectiles, overestimating the experimental data significantly except at very high energies (around 1 MeV and higher). For antiproton impact, the adiabatic correlation integral brings the double-removal cross-section close to the experimental data points (which tend to have large error bars).³ For protons, however, there remains a discrepancy larger than a factor of two over a wide impact energy range. The more detailed analysis carried out in [36] suggests that the WB model presents limitations in situations where capture is

Atoms 2024, 12, 31 14 of 25

an important reaction channel. Regardless of this, the single-removal cross-section (left panel of Figure 5) shows nice agreement with the experimental data over the entire energy range. For antiproton impact, the IEM and WB predictions are very similar and fare equally well in explaining the experimental data. Comparing the absolute scales of the single-and double-removal cross-sections, we are led to conclude that we should focus on the two-electron process in order to shed more light on the role of I_c .

With this in mind, let us now come back to the observation that the WB model tends to reduce two-electron removal. A more detailed analysis of the transition probabilities confirms that $I_c^{\rm WB} < 0$ (cf. Equation (35)) at *all* impact parameters and collision energies considered [36]. This raises the question of whether this feature can be understood on more general grounds. In lieu of a strict proof (which seems impossible in light of the somewhat heuristic nature of the WB model), we present a simplified argument.

The adiabatic densities that feed into g_c (38) in the WB model are defined in a piecewise manner for the two cases, namely, where the net removal (19) is between zero and one and where it is between one and two. Only the former case is relevant for singly-charged projectiles. The WB model assumes that

$$g_c(\mathbf{r}_1, \mathbf{r}_2, t_f) = \frac{2\rho^A(\mathbf{r}_1, \mathbf{r}_2, t_f)}{n^A(\mathbf{r}_1, t_f)n^A(\mathbf{r}_2, t_f)} - \frac{1}{2}$$
(40)

with

$$\rho^{A}(\mathbf{r}_{1}, \mathbf{r}_{2}, t_{f}) = (1 - P_{\text{net}}^{\text{rem}})\rho_{2}(\mathbf{r}_{1}, \mathbf{r}_{2}) = (1 - 2p)\rho_{2}(\mathbf{r}_{1}, \mathbf{r}_{2}), \tag{41}$$

where ρ_2 is the two-electron ground-state density of the (helium) atom, $0 \le p = P_{\text{net}}^{\text{rem}}/2 \le 1/2$, and

$$n^{A}(\mathbf{r}, t_{f}) = (1 - 2p)n_{2}(\mathbf{r}) + 2pn_{1}(\mathbf{r})$$
 (42)

with the ground-state densities n_2 of the two-electron helium atom and n_1 of the one-electron helium ion. If we make the additional assumptions that $\rho_2(\mathbf{r}_1, \mathbf{r}_2) = \frac{1}{4}n_2(\mathbf{r}_1)n_2(\mathbf{r}_2)$ and $n_1(\mathbf{r}) = \frac{1}{2}n_2(\mathbf{r})$, i.e., that the two-electron density of the neutral atom is uncorrelated and that the ground-state orbital of the singly-charged ion is identical to the (doubly-occupied) ground-state orbital of the atom, we arrive at

$$g_c = -\frac{p^2}{2(1-p)^2} \tag{43}$$

and

$$I_c = -2p^2 \equiv I_c^{\text{quadratic}},\tag{44}$$

i.e., a strictly negative correlation integral. However, the quadratic p dependence (44) is too extreme, in that it implies $P_2 = 0$ (cf. Equation (35)). We can relax it somewhat by writing (cf. Equation (36))

$$I_c = -\frac{1}{2}P_1^2 \tag{45}$$

and substituting the IEM probability (25) to obtain the quartic function

$$I_c^{\text{quartic}} = -2p^2 + 4p^3 - 2p^4. (46)$$

Alternatively, for small p it is justified to neglect the highest-order term to arrive at the cubic form

$$I_c^{\text{cubic}} = -2p^2 + 4p^3 \tag{47}$$

as a compromise. Both the quartic and cubic forms of I_c are negative for p < 1/2, just as is the case with I_c^{WB} ; in fact, when used to calculate the single- and double-removal cross-sections, they yield similar results to the WB model, as demonstrated in Figure 6. For antiproton impact (left panel), the cubic model's double ionization results are remarkably close to the WB cross-sections, while the quartic model produces a cross-section curve

Atoms 2024, 12, 31 15 of 25

that is similar in shape but visibly lower. For proton impact (right panel), on the other hand, the quartic model is in better overall agreement with the WB results than the cubic model. Either way, it is interesting to see that the obtained results are of similar quality to the numerically nontrivial WB model. Both the cubic and the quartic models are as easy to implement as the IEM.

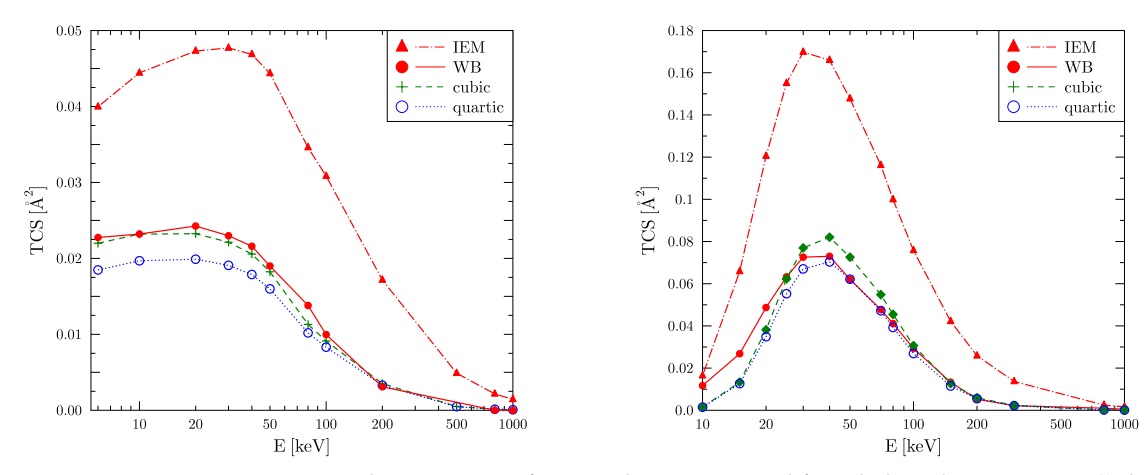


Figure 6. Total cross-section for two-electron removal from helium by antiproton (**left panel**) and proton (**right panel**) impact as functions of the collision energy. All results shown are obtained from the BGM calculations of [36] employing different final-state analyses. In addition to the IEM and WB data included in Figure 5, results when using Equations (47) ('cubic') and (46) ('quartic') are displayed.

From a more fundamental perspective, however, it must be conceded that the above-mentioned problem of a fixed relation between the single- and double-removal probabilities (cf. Equation (27)) remains unsolved; the cubic and quartic models merely replace the IEM relation by a different one, and given the similarity of cross-section results displayed in Figure 6, it must be concluded that the WB model does not offer more flexibility in practice. The two-electron calculations reported in Reference [32] indicate that such flexibility is needed in reality. In particular, it has been shown there that the correlation integral tends to be positive at relatively high impact energies, a feature that is clearly beyond the capabilities of the models discussed in this section. Looking at the (exact) expression (36), we can conclude that a model for both the first and second terms of I_c would be needed to replicate this behavior, involving at least one variable in addition to the effective single-electron probability p. Going back to Equations (33)–(35) and using $P_j \geq 0$ for j = 0, 1, 2 as conditions, it can easily be established that the allowed values of I_c in the $0 \leq p \leq 1$ domain fall within the encircled area⁴ shown in Figure 7.

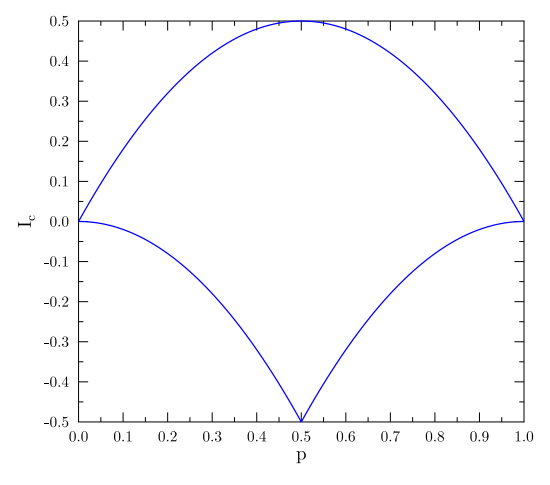


Figure 7. Correlation integral versus *p*; the allowed values fall within the encircled area.

Atoms 2024, 12, 31 16 of 25

Obviously, this leaves us with many viable options for modeling the correlation integral. Whether an improved model with more flexibility can be found without resorting to essentially fitting the target results is unknown at present.

3.3. Multiple Electron Processes in Collisions Involving Neon Atoms

The preceding discussion seems to suggest that we should not hope for the IEM to be able to explain multi-electron removal processes. While this is obviously true for protonhelium and antiprotonhelium collisions, the statement needs to be qualified when the projectile has a higher charge state and/or the target atom has more than two electrons. The He²⁺-Ne system represents an interesting case for demonstrating this. It was studied in [24] using the simple target response model and the BGM for orbital propagation. More recently, real-space finite-difference calculations at the ALDA level, including self-interaction corrections, were carried out in [61]. The Ehrenfest dynamics method was used to couple the motion of the nuclei to the electron dynamics, although it seems unlikely that this would cause any notable changes in the cross-section results compared to a calculation with straightline trajectories unless very low collision energies are considered. Another feature of the calculations reported in [61] involved the use of a so-called coordinate space translation technique to separately analyze the electronic states of projectile and target centers [62]. Similar techniques were used in a number of recent studies for many-electron systems [63–65], all of which used the Octopus code [66].

Figure 8 compares the total cross-sections for q-fold electron removal from neon obtained from both methods with each other and with experimental data. Different variants of IEM analyses were employed; in [24], a so-called products-of-binomials analysis designed to prevent unphysical higher-order electron capture was used, while [61] used an analysis based on Slater determinantal wave functions. Good overall agreement is observed in Figure 8 for both single (q=1) and double (q=2) electron removal. For q=3, the ALDA calculation from [61] is in better agreement with the measurements than the target response calculation at most energies, although it could be argued that the latter fares better in matching the energy dependence of the experimental data points. The same appears to be true for q=4, notwithstanding a substantial overestimation of the data by the calculations of [24] in the entire range of impact energies shown. The ALDA calculation, by contrast, overestimates the measurements only at low and intermediate impact energies, a tendency that is already visible for q=3.

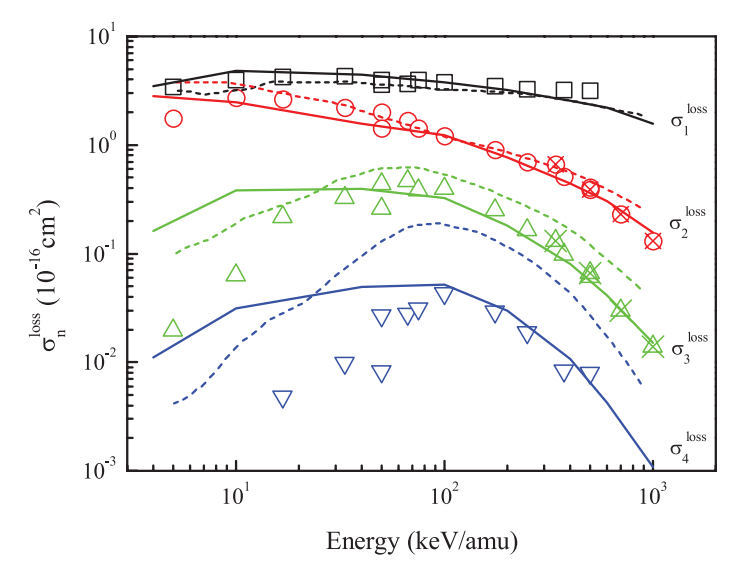


Figure 8. Total cross-sections for $q = 1, \dots 4$ -fold electron removal (termed 'loss' in the figure) from neon by He²⁺ impact as functions of collision energy. Theory: solid lines, ALDA [61], dashed lines, BGM response [24]. Experiments: open symbols [48], crosses with open symbols [67]. Reprinted from [61] with the permission of AIP Publishing.

Atoms 2024, 12, 31 17 of 25

Figure 9 shows a similar plot for ${\rm Li^{3+}}$ -Ne collisions, except that the cross-sections are for pure ionization, i.e., processes in which the projectile does not change its charge state. Again, the calculations are based on the target response model and the BGM; however, in this case a determinantal analysis similar to that used in [61] for ${\rm He^{2+}}$ was used instead of the products-of-binomials scheme.

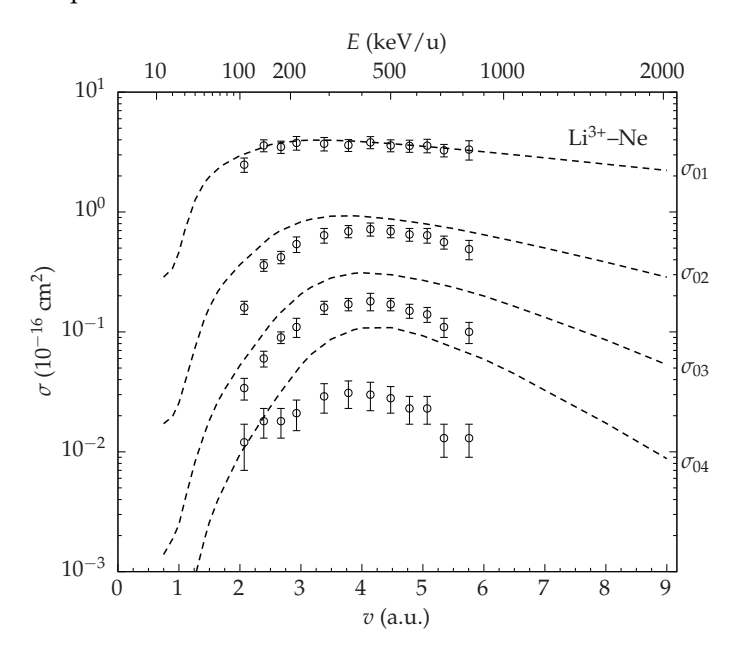


Figure 9. Total cross-sections for $q = 1, \dots 4$ -fold pure ionization of neon by Li^{3+} impact as functions of collision energy. Dashed lines, BGM response calculations [68]. Experiments: open circles [69]. Reproduced with permission from [70].

The agreement with the experimental data is excellent for q=1 and satisfactory for q=2. For q=3, similarly to the He²⁺ case, reasonable agreement can be claimed in shape but not in magnitude. For q=4, the calculated cross-sections are too high by at least a factor of three in the region of the peak, and the agreement observed for the two data points at the lowest energies appears fortuitous. It would be of interest to know how an ALDA calculation would fare for this problem, but such results have not been reported.

In any case, it appears fair to summarize the situation by saying that the IEM analysis of collision calculations works reasonably well as long as the final target charge state q does not exceed the initial projectile charge state (or, in certain circumstances, by not more than one). This has been confirmed in a number of works for various collision systems (see, e.g., [71] and references therein) and seems to be true regardless of the level of approximation employed for the TDKS potential. Thus, it can be concluded that an extended correlation integral model for N > 2 electrons would be required to obtain improved agreement with experiments at high charge states.

3.4. Collision Systems with Electrons on Both Centers

One of the simplest collision systems with active target and projectile electrons is the three-electron He⁺-He system. It was studied in [26] in the exchange-only limit of a time-dependent spin-density formalism. This level of theory ensures that each of the three electrons experiences the correct asymptotic potential at large distances, a feature which is important in collision problems and hard to achieve in simplified response or no-response models if electrons on both centers are present in the initial state. A few compromises needed to be accepted in [26] to make this work: (i) the KLI approximation was used instead of the full OPM to generate the exchange potential; and (ii) the potential was calculated with a cylindrical symmetry constraint, which in reality it does not possess for finite impact

Atoms 2024, 12, 31 18 of 25

parameter collisions. The final-state analysis was carried out at the level of the IEM with Slater determinantal wave functions for the three-electron system.

All charge-changing outcome channels were reported in [26]. Here, we focus on those that involve electron loss from the projectile, and only include the most sophisticated KLI calculation, labeled as pETF in [26], which takes into account a partial electron translation factor in the orbitals that feed into the effective potential.

Figure 10 displays the cross-section for single electron loss from the projectile with no simultaneous electron removal from the target. While the overall agreement with the measurements is quite good, an overestimation of the data can be noted at impact energies of 200 keV/amu and higher, in which region an independent event model calculation [72] matches the data very well. That calculation takes electron correlation effects into account explicitly. It is also included for comparison in Figures 11 and 12, which show projectile electron loss in coincidence with single and double target ionization, respectively.

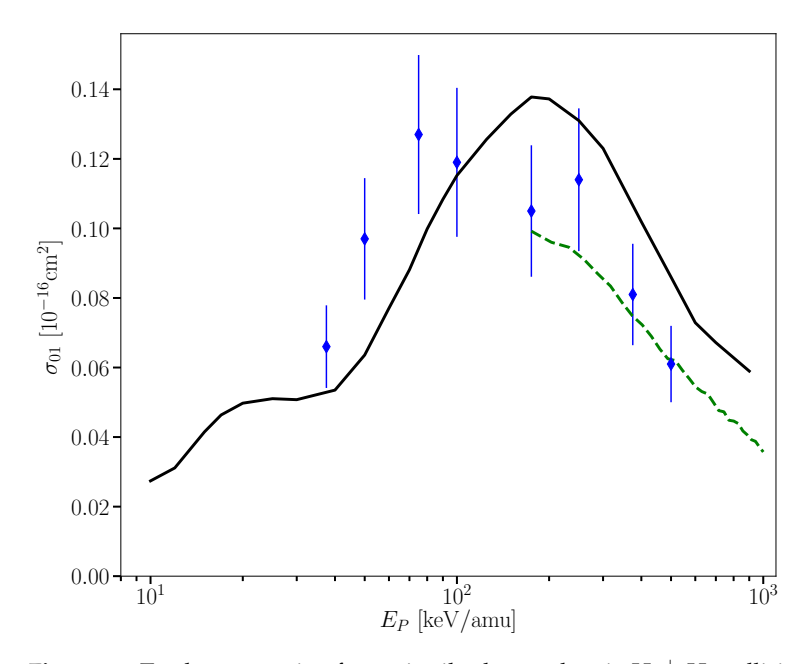


Figure 10. Total cross-section for projectile electron loss in He⁺-He collisions as a function of collision energy. Theory: solid line, KLI-IEM [26], dashed line, independent event model [72]. Experiments: diamonds [73]. Adapted from [26].

In the case of single target ionization (Figure 11), the situation appears reversed in that the results of the KLI-IEM calculation are below those of the independent event model and the experimental data at high impact energies. This is explained by a process that is sometimes referred to as antiscreening, which involves a direct interaction between a target and a projectile electron, resulting in their simultaneous ionization. The independent event calculation takes antiscreening into account, whereas the KLI-IEM calculation does not. It has been argued that the antiscreening process has an effective threshold determined by the condition that the kinetic energy of a (free) electron travelling with the relative projectile-target speed must be larger than the sum of the ionization potentials of both electrons. For He^+ -He collisions, this threshold would correspond to a collision energy of about $146 \, \text{keV/amu}$, which is consistent with the observation that the KLI-IEM calculation tends to grow closer to the experimental data of Figure 11 towards lower energies.

For double target ionization in coincidence with projectile electron loss (Figure 12), the fact that the KLI-IEM results are below the experimental data at the highest energies can be attributed to the same type of electron–electron correlation effect, which the independent event model calculation of [72] appears to overestimate in this channel. In the region of the cross-section peak, the KLI-IEM results are above the measurements, confirming the usual

Atoms 2024, 12, 31 19 of 25

trend that an IEM final-state analysis overestimates the charge-changing cross-sections for channels with high electron multiplicities.

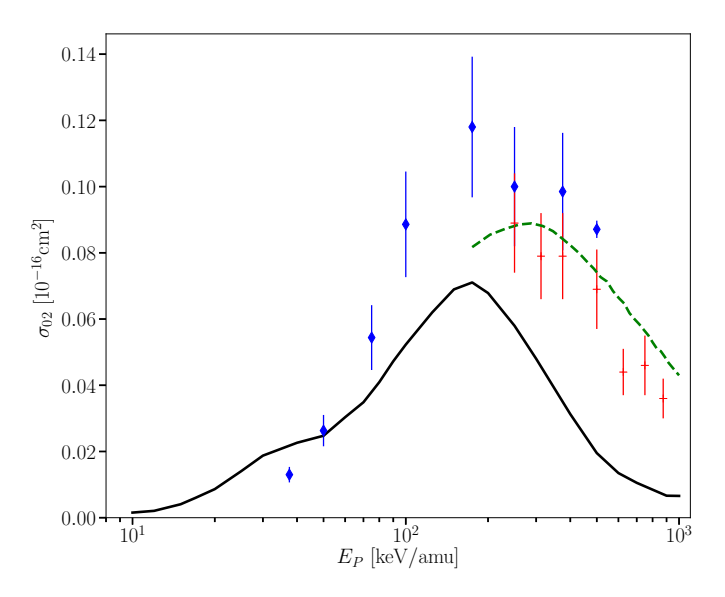


Figure 11. Total cross-section for projectile electron loss with single target ionization in He⁺-He collisions as a function of collision energy. Theory: solid line, KLI-IEM [26], dashed line, independent event model [72]. Experiments: diamonds [73], crosses [74]. Adapted from [26].

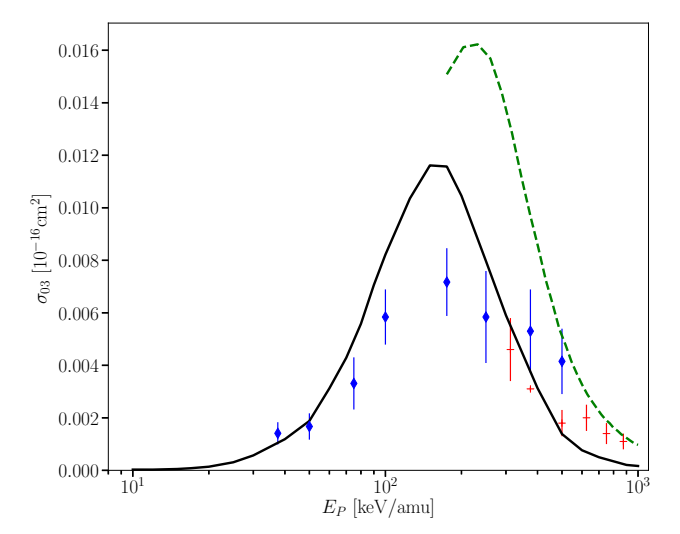


Figure 12. Total cross-section for projectile electron loss with double target ionization in He⁺-He collisions as a function of collision energy. Theory: solid line, KLI-IEM [26], dashed line, independent event model [72]. Experiments: diamonds [73], crosses [74]. Adapted from [26].

When taken together, it can be concluded that the three projectile electron loss channels are described quite well by the KLI-IEM calculation. An interesting question is whether a correlation integral model for this three-electron problem would be able to improve the description by way of reshuffling flux between the three channels, whether an improved TDKS potential would be required, or perhaps both. A viable ansatz for one or the other would be needed to shed light on this question.

We round this section off with a comment on a truly many-electron problem: the Ar⁺-Ne system, which was studied in a TDDFT framework in [75]. The level of theory used in that work is similar to that in [61] and other recent works for collision problems with target and projectile electrons [76,77]. In particular, the calculations were carried out at the ALDA level, with self-interaction corrections included and analyzed at the final time on the basis of Slater determinantal wave functions. A total of fifteen electrons were

Atoms **2024**, 12, 31 20 of 25

considered active, with the electrons in the $2s^22p^6$ configuration on the neon target atom and the $3s^23p^5$ electrons on the Ar^+ ion, while the inner shell electrons were frozen and accounted for via pseudopotentials.

Single-electron capture and $m=1,\ldots,5$ -fold electron loss cross-sections were reported in [75]. The level of agreement with experiment was found to be quite good, in particular at impact energies in the 25–45 keV/amu range. This is remarkable for electron loss at higher multiplicities m, given the IEM nature of the final-state analysis and the somewhat contradictory evidence gathered from other seemingly simpler collision systems (cf. Section 3.3). While the theoretical model may decrease in validity towards lower energies, as suggested by the authors of [75], conflicting capture measurements and a sparsity of electron loss data make it difficult to draw definitive conclusions in this region. Notwithstanding these uncertainties, the results can be deemed encouraging regarding the applicability of TDDFT to complex collision problems.

4. Conclusions and Outlook

Since its formal birth in 1984, TDDFT has found practical application in many areas, atomic collisions in the semiclassical framework being one of them. The appeal of TDDFT is that it is built on a provable theorem, the Runge–Gross theorem, on the basis of which it can be argued that the many-body TDSE can be replaced by a seemingly simpler effective single-particle description, the TDKS scheme. Practical calculations are, however, necessarily of an approximate nature, as (i) the exact form of the TDKS potential is unknown and (ii) the exact density dependence of many observables of interest is unknown as well. Although progress has been made on both fronts, there are outstanding questions that need answers if TDDFT calculations are to significantly transcend the IEM level.

Regarding the TDKS potential, 'exact' exchange-only calculations, i.e., attempts at numerically solving the equations one encounters when neglecting correlation but including exchange exactly, have been reported for only the simplest (true or effective two-electron) collision systems. For more general situations, the OPM provides a framework for formulating the problem; however, a complicated integral equation needs to be solved in order to generate the exact exchange potential. To the best of our knowledge, this has not been attempted yet for atomic collision problems. Even applications of the simpler KLI scheme are scarce, and subject to further approximations in practice. The bulk of the numerical results generated thus far are either based on local density type approximations or even simpler global response (and no-response) models. This is to say that not much is known about the role of the correlation contribution to the TDKS potential. Static correlation, i.e., a no-response type inclusion of atomic ground-state contributions, was found to be unimportant for collisions involving helium atoms, but it should not be concluded from this that time-dependent effects will be small as well. Some time ago, the application of a simple time-dependent correlation potential model originally developed for laser-atom interactions [78] showed effects in the antiproton-helium system; however, this did not lead to improvements compared to the IEM, and was dismissed as unsuitable for the collision problem [79]. Progress has been made regarding understanding the properties of the exact TDKS potential, and, as a consequence, of time-dependent correlation effects on a formal level and for model problems (see, e.g., [80,81] and references therein). One lesson learned from these studies concerns the memory dependence of the exact TDKS potential, i.e., a dependence of the potential at time t on the density at times t' < t (and the initial state). While this dependence appears to be important in general, it is usually neglected in practice. It remains to be seen whether workable models for approximate inclusion of memory effects can be developed and applied to collision problems.

The problem of correlation in the final-state analysis has been discussed in some detail in this article. Existing models for a correlation integral to describe (single- and) double-capture and ionization events in two-electron systems have led to encouraging results, but require further improvements in order to make TDDFT-based approaches competitive with explicit two-electron calculations. For problems with N>2 electrons, for which explicit

Atoms 2024, 12, 31 21 of 25

calculations become prohibitively costly with increasing N, viable correlation integral models do not currently exist. It might be useful to direct effort into their development in order to shed light on the issue of high electron multiplicities in ionizing collisions (see the discussion in Section 3.3). Such progress would also benefit neighboring research areas, such as the study of laser—atom interactions, in which high degrees of ionization can be reached in intense fields and where TDDFT methods play at least as important a role as in the collision field.

This article has focused on collisions with *atomic* targets and discussed the accomplishments and limitations of TDDFT-based calculations on the basis of *total* cross-section results; however, there is also considerable interest in collisions involving molecules as well as in differential cross-section studies, making a few comments from the TDDFT perspective in order here.

Differential studies again raise the question of how to express the observables of interest in terms of the density. In the apparent absence of a known direct approach, an analysis based on the individual orbitals, i.e., at the level of the IEM, seems to be the only available option at present. There is a case to be made that some attention should be devoted to this problem.

More can be said about the study of collisions involving molecules. A number of TDDFT calculations, many of them using the Octopus code [66] and combining the TDKS equations with the Ehrenfest dynamics method to account for the motion of the nuclei, have been carried out to date [42,82–93]. The difficulty of addressing the complicated ion–molecule problem with explicit many-body methods, coupled with the many successes of stationary density functional theory in the quantum chemistry realm, makes this area a natural field for TDDFT and simplified TDDFT-inspired approaches. Further progress in the description of ion–atom collisions along the lines indicated above will benefit the study of molecular systems as well. In light of the applied interest in this area, it seems safe to predict increased TDDFT activity in the coming years.

Funding: This work has been supported by the Natural Sciences and Engineering Research Council of Canada (NSERC) (RGPIN-2019-06305).

Conflicts of Interest: The author declares no conflicts of interest.

Abbreviations

The following abbreviations are used in this manuscript:

ALDA Adiabatic Local Density Approximation
BGM Basis Generator Method

CCC Convergent Close Coupling
DFT Density Functional Theory
IEM Independent Electron Model

KLI Krieger-Li-Iafrate

OPM Optimized Potential Method pETF partial Electron Translation Factor

SC-CCC Semiclassical Convergent Close Coupling TDDFT Time-Dependent Density Functional Theory

TDHF Time-Dependent Hartree–Fock TDKS Time-Dependent Kohn–Sham

TDSE Time-Dependent Schrödinger Equation

WB Wilken-Bauer

Notes

- One actually needs the so-called van Leeuwen theorem to ensure that it is possible to replace the interacting system with a fictitious noninteracting system that reproduces the exact density [18].
- The energy loss contributions from projectile–nucleus target–nucleus scattering are known to be relatively small at sufficiently high collision energies; see the discussion in [27].

Atoms **2024**, 12, 31 22 of 25

State-of-the-art correlated two-electron calculations yield a different energy dependence compared to the WB model and appear to be in better agreement with the experimental data; see, e.g., [32,49] and references cited therein.

 $P_i \le 1$ turn out to be weaker conditions in this representation, i.e., they do not play a role in determining the allowed I_c area.

References

- 1. Runge, E.; Gross, E.K.U. Density-Functional Theory for Time-Dependent Systems. Phys. Rev. Lett. 1984, 52, 997. [CrossRef]
- 2. Kirchner, T.; Gulyás, L.; Lüdde, H.J.; Engel, E.; Dreizler, R.M. Influence of electronic exchange on single and multiple processes in collisions between bare ions and noble-gas atoms. *Phys. Rev. A* **1998**, *58*, 2063. [CrossRef]
- 3. Saalmann, U.; Schmidt, R. Excitation and Relaxation in Atom-Cluster Collisions. Phys. Rev. Lett. 1998, 80, 3213–3216. [CrossRef]
- 4. Yabana, K.; Tazawa, T.; Abe, Y.; Bożek, P. Time-dependent mean-field description for multiple electron transfer in slow ion-cluster collisions. *Phys. Rev. A* **1998**, *57*, R3165–R3168. [CrossRef]
- 5. Nagano, R.; Yabana, K.; Tazawa, T.; Abe, Y. Application of the time-dependent local density approximation to collision between a highly charged ion and an atom. *J. Phys. B At. Mol. Opt. Phys.* **1999**, *32*, L65. [CrossRef]
- 6. Ullrich, C.A.; Gossmann, U.J.; Gross, E.K.U. Density-Functional Approach to Atoms in Strong Laser Pulses. *Berichte Der Bunsenges. Für Phys. Chem.* **1995**, *99*, 488–497. [CrossRef]
- 7. Ullrich, C.A.; Erhard, S.; Gross, E.K.U. Density-functional approach to atoms in strong laser pulses. In *Super Intense Laser Atom Physics IV*; Muller, H.G., Fedorov, M.V., Eds.; Kluwer: Dordrecht, The Netherlands, 1996; pp. 267–284.
- 8. Ullrich, C.A.; Gross, E.K.U. Many-Electron Atoms in Strong Femtosecond Laser Pulses: A Density-Functional Study. *Comments At. Mol. Phys.* **1997**, *33*, 211–236.
- 9. Tong, X.M.; Chu, S.I. Time-dependent density-functional theory for strong-field multiphoton processes: Application to the study of the role of dynamical electron correlation in multiple high-order harmonic generation. *Phys. Rev. A* **1998**, *57*, 452–461. [CrossRef]
- 10. Hill, C.; Dipti.; Heinola, K.; Dubois, A.; Sisourat, N.; Taoutioui, A.; Agueny, H.; Tőkési, K.; Ziaeian, I.; Illescas, C.; et al. Atomic collisional data for neutral beam modeling in fusion plasmas. *Nucl. Fusion* **2023**, *63*, 125001. [CrossRef]
- 11. Ullrich, J.; Shevelko, V.P. (Eds.) *Many-Particle Quantum Dynamics in Atomic and Molecular Fragmentation*; Springer Series on Atomic, Optical, and Plasma Physics; Springer: Berlin/Heidelberg, Germany, 2003; Volume 35. [CrossRef]
- 12. Marques, M.A.L.; Maitra, N.T.; Nogueira, F.M.S.; Gross, E.K.U.; Rubio, A. (Eds.) *Fundamentals of Time-Dependent Density Functional Theory*; Lecture Notes in Physics; Springer: Berlin/Heidelberg, Germany, 2012; Volume 837. [CrossRef]
- 13. Ullrich, C.A. *Time-Dependent Density-Functional Theory: Concepts and Applications*; Oxford University Press: Oxford, UK, 2012. [CrossRef]
- 14. Marques, M.A.L.; Gross, E.K.U. Time-Dependent Density Functional Theory. Annu. Rev. Phys. Chem. 2004, 55, 427. [CrossRef]
- 15. Sisourat, N.; Dubois, A. Semiclassical close-coupling approaches. In *Ion-Atom Collisions: The Few-Body Problem in Dynamic Systems*; Schulz, M., Ed.; De Gruyter: Berlin, Germany, 2019; pp. 157–178. [CrossRef]
- 16. Laoutaris, A.; Nanos, S.; Biniskos, A.; Passalidis, S.; Benis, E.P.; Dubois, A.; Zouros, T.J.M. Projectile excitation to autoionizing states in swift collisions of open-shell He-like ions with helium. *Phys. Rev. A* **2024**, *109*, 032825. [CrossRef]
- 17. Kirchner, T.; Ford, A.L.; Reading, J.F. Ion-Atom and Atom-Atom Collisions. In *Springer Handbook of Atomic, Molecular, and Optical Physics*; Drake, G.W.F., Ed.; Springer: Cham, Switzerland, 2023; pp. 785–794. [CrossRef]
- 18. van Leeuwen, R. Mapping from Densities to Potentials in Time-Dependent Density-Functional Theory. *Phys. Rev. Lett.* **1999**, 82, 3863. [CrossRef]
- 19. Engel, E. Orbital-Dependent Functionals for the Exchange-Correlation Energy: A Third Generation of Density Functionals. In *A Primer in Density Functional Theory*; Fiolhais, C., Nogueira, F., Marques, M.A.L., Eds.; Springer: Berlin/Heidelberg, Germany, 2003; pp. 56–122. [CrossRef]
- 20. Kümmel, S.; Kronik, L. Orbital-dependent density functionals: Theory and applications. *Rev. Mod. Phys.* **2008**, *80*, 3–60. [CrossRef]
- 21. Ullrich, C.A.; Gossmann, U.J.; Gross, E.K.U. Time-Dependent Optimized Effective Potential. *Phys. Rev. Lett.* **1995**, 74, 872–875. [CrossRef]
- 22. Krieger, J.; Li, Y.; Iafrate, G. Derivation and application of an accurate Kohn-Sham potential with integer discontinuity. *Phys. Lett. A* **1990**, *146*, 256–260. [CrossRef]
- 23. de Faria, J.C.; Santiago, J.; Francis, Z.; Bernal, M.A. Time-Dependent Density-Functional Theory for Determining the Electron-Capture Cross Section for Protons Impacting on Atoms and Molecules. *J. Phys. Chem. A* **2023**, 127, 2453–2459. [CrossRef]
- 24. Kirchner, T.; Horbatsch, M.; Lüdde, H.J.; Dreizler, R.M. Time-dependent screening effects in ion-atom collisions with many active electrons. *Phys. Rev. A* **2000**, *62*, 042704. [CrossRef]
- 25. Kirchner, T.; Horbatsch, M.; Lüdde, H.J. Nonperturbative calculation of charge-changing processes in C⁴⁺ scattering from neon atoms. *Phys. Rev. A* **2001**, *64*, 012711. [CrossRef]
- 26. Baxter, M.; Kirchner, T.; Engel, E. Time-dependent spin-density-functional-theory description of He⁺-He collisions. *Phys. Rev. A* **2017**, *96*, 032708. [CrossRef]
- 27. Lüdde, H.J.; Horbatsch, M.; Kirchner, T. Calculation of energy loss in antiproton collisions with many-electron systems using Ehrenfest's theorem. *Phys. Rev. A* **2021**, *104*, 032813. [CrossRef]

Atoms 2024, 12, 31 23 of 25

28. Lüdde, H.J. Time-Dependent Density Functional Theory in Atomic Collisions. In *Many-Particle Quantum Dynamics in Atomic and Molecular Fragmentation*; Ullrich, J., Shevelko, V.P., Eds.; Springer: Berlin/Heidelberg, Germany, 2003; pp. 205–220. [CrossRef]

- 29. Löwdin, P.O. Quantum Theory of Many-Particle Systems. I. Physical Interpretations by Means of Density Matrices, Natural Spin-Orbitals, and Convergence Problems in the Method of Configurational Interaction. *Phys. Rev.* **1955**, *97*, 1474–1489. [CrossRef]
- 30. Lüdde, H.J.; Horbatsch, M.; Kirchner, T. Independent-atom-model description of multiple ionization of water, methane, and ammonia molecules by proton impact. *Phys. Rev. A* **2022**, *106*, 022813. [CrossRef]
- 31. Baxter, M.; Kirchner, T. Correlation in time-dependent density-functional-theory studies of antiproton-helium collisions. *Phys. Rev. A* **2013**, *87*, 062507. [CrossRef]
- 32. Jia, C.C.; Kirchner, T.; Gao, J.W.; Wu, Y.; Wang, J.G.; Sisourat, N. Single- and double-ionization processes of antiproton-helium and antiproton-molecular hydrogen collisions in the keV energy range. *Phys. Rev. A* **2023**, *107*, 012808. [CrossRef]
- 33. Petersilka, M.; Gross, E.K.U. Strong-field double ionization of helium: A density-functional perspective. *Laser Phys.* **1999**, *9*, 105–114.
- 34. de Wijn, A.S.; Kümmel, S.; Lein, M. Numerical aspects of real-space approaches to strong-field electron dynamics. *J. Comput. Phys.* **2007**, 226, 89–103. [CrossRef]
- 35. Wilken, F.; Bauer, D. Adiabatic Approximation of the Correlation Function in the Density-Functional Treatment of Ionization Processes. *Phys. Rev. Lett.* **2006**, 97, 203001. [CrossRef]
- 36. Baxter, M.; Kirchner, T. Time-dependent density-functional-theory studies of collisions involving He atoms: Extension of an adiabatic correlation-integral model. *Phys. Rev. A* **2016**, *93*, 012502. [CrossRef]
- 37. Wang, F.; Zhang, K.; Mao, F.; Wang, J. Calculation of electron capture probability of energetic protons colliding with rare-gas atoms: A comparison study on four methods. *Chem. Phys.* **2021**, *541*, 111035. [CrossRef]
- 38. Kroneisen, O.J.; Lüdde, H.J.; Kirchner, T.; Dreizler, R.M. The basis generator method: Optimized dynamical representation of the solution of time-dependent quantum problems. *J. Phys. A Math. Gen.* **1999**, 32, 2141. [CrossRef]
- 39. Bailey, J.J.; Kadyrov, A.S.; Abdurakhmanov, I.B.; Fursa, D.V.; Bray, I. Antiproton stopping in atomic targets. *Phys. Rev. A* **2015**, 92, 022707. [CrossRef]
- 40. Keim, M.; Achenbach, A.; Lüdde, H.; Kirchner, T. Time-dependent density functional theory calculations for collisions of bare ions with helium. *Nucl. Instrum. Methods Phys. Res. Sect. B Beam Interact. Mater. At.* **2005**, 233, 240–243. [CrossRef]
- 41. Zhao, S.; Kang, W.; Xue, J.; Zhang, X.; Zhang, P. H⁺ (D⁺, T⁺)-beryllium collisions studied using time-dependent density functional theory. *Phys. Lett. A* **2015**, *379*, 319–326. [CrossRef]
- 42. Avendaño-Franco, G.; Piraux, B.; Grüning, M.; Gonze, X. Time-dependent density functional theory study of charge transfer in collisions. *Theor. Chem. Acc.* **2012**, *131*, 1289. [CrossRef]
- 43. Wang, F.; Yao, Y.; Calvayrac, F.; Zhang, F. Extraction of state-resolved information from systems with a fractional number of electrons within the framework of time-dependent density functional theory. *J. Chem. Phys.* **2016**, *145*, 114104. [CrossRef]
- 44. Rudd, M.E.; DuBois, R.D.; Toburen, L.H.; Ratcliffe, C.A.; Goffe, T.V. Cross sections for ionization of gases by 5-4000-keV protons and for electron capture by 5-150-keV protons. *Phys. Rev. A* **1983**, *28*, 3244–3257. [CrossRef]
- 45. Rudd, M.E.; Kim, Y.K.; Madison, D.H.; Gallagher, J.W. Electron production in proton collisions: Total cross sections. *Rev. Mod. Phys.* **1985**, *57*, 965–994. [CrossRef]
- 46. Rudd, M.E.; Goffe, T.V.; Itoh, A. Ionization cross sections for 10–300-keV/u and electron-capture cross sections for 5–150-keV/u ³He²⁺ ions in gases. *Phys. Rev. A* **1985**, *32*, 2128–2133. [CrossRef]
- 47. DuBois, R.D. Ionization and charge transfer in He²⁺-rare-gas collisions. *Phys. Rev. A* 1986, 33, 1595–1601. [CrossRef]
- 48. DuBois, R.D. Ionization and charge transfer in He²⁺-rare-gas collisions. II. *Phys. Rev. A* 1987, 36, 2585–2593. [CrossRef]
- 49. Borbély, S.; Feist, J.; Tőkési, K.; Nagele, S.; Nagy, L.; Burgdörfer, J. Ionization of helium by slow antiproton impact: Total and differential cross sections. *Phys. Rev. A* **2014**, *90*, 052706. [CrossRef]
- 50. Barna, I.F.; Pocsai, M.A.; Tőkési, K. Ab Initio Double-Differential Ionization Cross-Section Calculations in Antiproton–Helium Collisions. *Atoms* **2023**, *11*, 74. [CrossRef]
- 51. DuBois, R.D.; Toburen, L.H.; Rudd, M.E. Multiple ionization of rare gases by H⁺ and He⁺ impact. *Phys. Rev. A* **1984**, 29, 70–76. [CrossRef]
- 52. Solovev, E.S.; Ilin, R.N.; Oparin, V.A.; Fedorenko, N.V. Ionization of gases by fast hydrogen atoms and by protons. *Sov. Phys. JETP-USSR* **1962**, *15*, 459.
- 53. Shah, M.B.; McCallion, P.; Gilbody, H.B. Electron capture and ionisation in collisions of slow H⁺ and He²⁺ ions with helium. *J. Phys. B At. Mol. Opt. Phys.* **1989**, 22, 3037. [CrossRef]
- 54. Shah, M.B.; Gilbody, H.B. Single and double ionisation of helium by H⁺, He²⁺ and Li³⁺ ions. *J. Phys. B At. Mol. Phys.* **1985**, 18, 899. [CrossRef]
- 55. Puckett, L.J.; Martin, D.W. Analysis of Recoil He⁺ and He⁺⁺ Ions Produced by Fast Protons in Helium Gas. *Phys. Rev. A* **1970**, 1,1432–1439. [CrossRef]
- 56. Wexler, S. Partial Ionization Cross Sections for Noble Gases Bombarded with 0.8–3.75-MeV Protons. *J. Chem. Phys.* **1964**, 41, 1714–1719. [CrossRef]
- 57. Knudsen, H.; Andersen, L.H.; Hvelplund, P.; Astner, G.; Cederquist, H.; Danared, H.; Liljeby, L.; Rensfelt, K.G. An experimental investigation of double ionisation of helium atoms in collisions with fast, fully stripped ions. *J. Phys. B At. Mol. Phys.* **1984**, 17, 3545. [CrossRef]

Atoms 2024, 12, 31 24 of 25

58. Knudsen, H.; Kristiansen, H.P.E.; Thomsen, H.D.; Uggerhøj, U.I.; Ichioka, T.; Møller, S.P.; Hunniford, C.A.; McCullough, R.W.; Charlton, M.; Kuroda, N.; et al. Ionization of Helium and Argon by Very Slow Antiproton Impact. *Phys. Rev. Lett.* **2008**, 101, 043201. [CrossRef]

- 59. Hvelplund, P.; Knudsen, H.; Mikkelsen, U.; Morenzoni, E.; Møller, S.P.; Uggerhøj, E.; Worm, T. Ionization of helium and molecular hydrogen by slow antiprotons. *J. Phys. B At. Mol. Opt. Phys.* **1994**, 27, 925. [CrossRef]
- 60. Andersen, L.H.; Hvelplund, P.; Knudsen, H.; Møller, S.P.; Pedersen, J.O.P.; Tang-Petersen, S.; Uggerhøj, E.; Elsener, K.; Morenzoni, E. Single ionization of helium by 40–3000-keV antiprotons. *Phys. Rev. A* **1990**, *41*, 6536–6539. [CrossRef]
- 61. Hong, X.; Wang, F.; Jiao, Y.; Su, W.; Wang, J.; Gou, B. Theoretical investigation of the electron capture and loss processes in the collisions of He²⁺ + Ne. *J. Chem. Phys.* **2013**, *139*, 084321. [CrossRef]
- 62. Wang, F.; Hong, X.; Wang, J.; Kim, K.S. Coordinate space translation technique for simulation of electronic process in the ion–atom collision. *J. Chem. Phys.* **2011**, 134, 154308. [CrossRef]
- 63. Wang, F.; Xu, X.; Hong, X.; Wang, J.; Gou, B. A theoretical model for electron transfer in ion–atom collisions: Calculations for the collision of a proton with an argon atom. *Phys. Lett. A* **2011**, 375, 3290–3295. [CrossRef]
- 64. Wang, F.; Hong, X.; Wang, J.; Gou, B.; Wang, J. Comparison of three methods for calculation of electron transfer probability in H⁺+Ne. *Phys. Lett. A* **2012**, *376*, 469–471. [CrossRef]
- 65. Zhang, C.L.; Hong, X.H.; Wang, F.; Wu, Y.; Wang, J.G. Theoretical investigation of He²⁺-Ar collisions in the energy range of 4–300 keV/amu. *Phys. Rev. A* **2013**, *87*, 032711. [CrossRef]
- 66. Andrade, X.; Strubbe, D.; De Giovannini, U.; Larsen, A.H.; Oliveira, M.J.T.; Alberdi-Rodriguez, J.; Varas, A.; Theophilou, I.; Helbig, N.; Verstraete, M.J.; et al. Real-space grids and the Octopus code as tools for the development of new simulation approaches for electronic systems. *Phys. Chem. Chem. Phys.* **2015**, *17*, 31371–31396. [CrossRef]
- 67. Andersen, L.H.; Hvelplund, P.; Knudsen, H.; Møller, S.P.; Sørensen, A.H.; Elsener, K.; Rensfelt, K.G.; Uggerhøj, E. Multiple ionization of He, Ne, and Ar by fast protons and antiprotons. *Phys. Rev. A* **1987**, *36*, 3612–3629. [CrossRef]
- 68. Schenk, G.; Kirchner, T. Multiple ionization of neon atoms in collisions with bare and dressed ions: A mean-field description considering target response. *Phys. Rev. A* **2015**, *91*, 052712. [CrossRef]
- 69. Ihani, J.S.; Luna, H.; Wolff, W.; Montenegro, E.C. Multiple ionization of neon induced by Li³⁺ and C³⁺ projectiles: Influence of projectile screening in the ionization and electron capture channels. *J. Phys. B At. Mol. Opt. Phys.* **2013**, *46*, 115208. [CrossRef]
- 70. Schenk, G. On the Role of Projectile Electrons in an Independent Electron Model Description of Dressed-Ion Impact on Atoms. Ph.D. Thesis, York University, Toronto, ON, Canada, 2016.
- 71. Schenk, G.; Horbatsch, M.; Kirchner, T. Role of projectile electrons for target-recoil-charge-state production in intermediate-energy B²⁺-Ne collisions. *Phys. Rev. A* **2013**, *88*, 012712. [CrossRef]
- 72. Sigaud, G.M.; Montenegro, E.C. Two-center electron-electron correlation within the independent event model. *Braz. J. Phys.* **2003**, 33, 382–391. [CrossRef]
- 73. DuBois, R.D. Multiple ionization in He⁺-rare-gas collisions. *Phys. Rev. A* **1989**, 39, 4440–4450. [CrossRef]
- 74. Santos, A.C.F.; Sigaud, G.M.; Melo, W.S.; Sant'Anna, M.M.; Montenegro, E.C. Absolute cross sections for projectile electron loss accompanied by target multiple ionization in collisions of He⁺ with noble gases. *J. Phys. B At. Mol. Opt. Phys.* **2011**, 44, 045202. [CrossRef]
- 75. Qin, S.; Gao, C.Z.; Yu, W.; Qu, Y.Z. Multi-Electron Transfer of Ar⁺ Colliding with Ne Atoms Based on a Time-Dependent Density-Functional Theory. *Chin. Phys. Lett.* **2021**, *38*, 063101. [CrossRef]
- 76. Yu, W.; Gao, C.Z.; Sato, S.A.; Castro, A.; Rubio, A.; Wei, B. Single and double charge transfer in the Ne²⁺ + He collision within time-dependent density-functional theory. *Phys. Rev. A* **2021**, *103*, 032816. [CrossRef]
- 77. Zhang, H.H.; Yu, W.D.; Gao, C.Z.; Qu, Y.Z. A Time-Dependent-Density-Functional-Theory Study of Charge Transfer Processes of Li²⁺ Colliding with Ar in the MeV Region. *Chin. Phys. Lett.* **2023**, *40*, 043101. [CrossRef]
- 78. Lein, M.; Kümmel, S. Exact Time-Dependent Exchange-Correlation Potentials for Strong-Field Electron Dynamics. *Phys. Rev. Lett.* **2005**, *94*, 143003. [CrossRef]
- 79. Henkel, N.; Keim, M.; Lüdde, H.J.; Kirchner, T. Density-functional-theory investigation of antiproton-helium collisions. *Phys. Rev.* A 2009, 80, 032704. [CrossRef]
- 80. Maitra, N.T. Perspective: Fundamental aspects of time-dependent density functional theory. *J. Chem. Phys.* **2016**, 144, 220901. [CrossRef]
- 81. Lacombe, L.; Maitra, N.T. Non-adiabatic approximations in time-dependent density functional theory: Progress and prospects. *Npj Comput. Mater.* **2023**, *9*, 124. [CrossRef]
- 82. Wang, Z.; Dinh, P.; Reinhard, P.G.; Suraud, E.; Bruny, G.; Montano, C.; Feil, S.; Eden, S.; Abdoul-Carime, H.; Farizon, B.; et al. Microscopic studies of atom-water collisions. *Int. J. Mass Spectrom.* **2009**, 285, 143–148. [CrossRef]
- 83. Gao, C.Z.; Wang, J.; Wang, F.; Zhang, F.S. Theoretical study on collision dynamics of H⁺ + CH₄ at low energies. *J. Chem. Phys.* **2014**, *140*, 054308. [CrossRef]
- 84. Hong, X.; Wang, F.; Wu, Y.; Gou, B.; Wang, J. H⁺ H₂O collisions studied by time-dependent density-functional theory combined with the molecular dynamics method. *Phys. Rev. A* **2016**, *93*, 062706. [CrossRef]
- 85. Quashie, E.E.; Saha, B.C.; Andrade, X.; Correa, A.A. Self-interaction effects on charge-transfer collisions. *Phys. Rev. A* **2017**, 95, 042517. [CrossRef]

Atoms **2024**, 12, 31 25 of 25

86. Covington, C.; Hartig, K.; Russakoff, A.; Kulpins, R.; Varga, K. Time-dependent density-functional-theory investigation of the collisions of protons and *α* particles with uracil and adenine. *Phys. Rev. A* **2017**, *95*, 052701. [CrossRef]

- 87. Seraide, R.; Bernal, M.A.; Brunetto, G.; de Giovannini, U.; Rubio, A. TDDFT-Based Study on the Proton–DNA Collision. *J. Phys. Chem. B* **2017**, *121*, 7276–7283. [CrossRef]
- 88. Zhao, R.T.; Zhang, N.; Zhang, F.S. Theoretical study on collision dynamics of H⁺ + H₂O at low energies. *Mol. Phys.* **2018**, 116, 231–241. [CrossRef]
- 89. Yu, W.; Gao, C.Z.; Zhang, Y.; Zhang, F.S.; Hutton, R.; Zou, Y.; Wei, B. Collision cross sections of N₂ by H⁺ impact at keV energies within time-dependent density-functional theory. *Phys. Rev. A* **2018**, *97*, 032706. [CrossRef]
- 90. Yu, W.; Gao, C.Z.; Jiang, T.; Zou, Y.; Wang, J.G.; Wu, Y.; Wei, B. A theoretical study of Ar⁸⁺-acetylene collisions at 1.2 MeV: Ionization and dissociation dynamics. *J. Chem. Phys.* **2019**, *150*, 124304. [CrossRef]
- 91. Wang, Z.; Zhang, F.; Xu, X.; Wang, Y.; Qian, C. Collision dynamics of proton to water dimer at 250 eV. *Mod. Phys. Lett. B* **2019**, 33, 1950257. [CrossRef]
- 92. Wang, Z.P.; Zhang, F.S.; Xu, X.F.; Qian, C.Y. Theoretical investigations of collision dynamics of cytosine by low-energy (150–1000 eV) proton impact. *Chin. Phys. B* **2020**, 29, 023401. [CrossRef]
- 93. Wang, X.; Wang, Z.P.; Zhang, F.S.; Qian, C.Y. Collision site effect on the radiation dynamics of cytosine induced by proton. *Chin. Phys. B* **2022**, *31*, 063401. [CrossRef]

Disclaimer/Publisher's Note: The statements, opinions and data contained in all publications are solely those of the individual author(s) and contributor(s) and not of MDPI and/or the editor(s). MDPI and/or the editor(s) disclaim responsibility for any injury to people or property resulting from any ideas, methods, instructions or products referred to in the content.